

Real-time Simulation of High-speed Flywheel Energy Storage System (FESS) for Low Voltage Networks

Shahab Karrari, Mathias Noe, Joern Geisbuesch
Institute of Technical Physics (ITEP)
Karlsruhe Institute of Technology (KIT)
Karlsruhe, Germany

Abstract— Real-time simulation of power system transients inevitably demands computation time steps of the order of microseconds or even less. This enables Power-Hardware-in-the-Loop (PHIL) testing of new power system components, such as innovative energy storage systems, which is an efficient cost-effective method to analyze the behavior of the component, prior to the grid connection. Having accurate real-time simulation models of the components is an essential step, prior to the PHIL testing. The new-generation Flywheel Energy Storage System (FESS), which uses High-Temperature Superconductors (HTS) for magnetic levitation and stabilization, is a novel energy storage technology. Due to quick response times, high power densities and high number of charging/discharging cycles, this new-generation FESS is especially suitable for enhancing power quality and transient stability in power systems. In this paper, the modeling and implementation of a FESS with HTS bearings in a real-time simulation environment are presented. The obtained real-time simulation results confirm the effectiveness of using such a FESS for improving power quality, e.g. voltage sag compensation in distribution networks and supporting the grid during frequency disturbances.

Index Terms—Real-time Simulation, Flywheel Energy Storage System, Energy Storage Systems, Power Quality.

I. INTRODUCTION

In the last decades, real-time simulators have gained more and more attention, as they are getting more cost-efficient and accurate with greater computational power. These simulators solve the differential equations that govern a system in simulation steps of the order of microseconds and even nanoseconds, in case of FPGA-based simulators [1]. This is achieved using a precompiled code, special solvers, and parallel processing. This accelerates the simulation of large power systems and in particular, the ones with a great share of Distributed Energy Resources (DER). Real-time simulation also grants the possibility of Power Hardware-in-the-Loop (PHIL) testing, as a cost-effective, safe and efficient means to test new power system equipment and innovative technologies under various operational scenarios. In fact, researchers have argued that PHIL will likely become the de facto tool for such purposes, in particular regarding grid integration of DER [2].

Nowadays, power systems face major challenges such as the increasing penetration of renewable energy resources in electrical systems, high power quality, and reliability expectations, and an increasing energy demands during the

peak hours. Therefore, the need for Energy Storage Systems (ESS) has escalated, in particular in the Transmission and Distribution (T&D) sector. According to a report by the International Energy Agency (IEA), 310 GW of additional grid-connected ESS is needed in the United States, Europe, China, and India to transform the energy sector over the next 40 years according to the plans [3].

Flywheel Energy Storage Systems (FESS) can contribute to frequency and voltage regulation, due to its quick response, high power density, high reliability, long lifetime, and an unlimited number of charging/discharging cycles (independent from the depth of discharge). Moreover, they can also take up the role of spinning reserve and provide energy for a black start, load leveling, ride through support, and unbalanced load compensation. The application of FESS in power systems is commonly investigated in association with grid-connected wind farms [4]–[8] for smoothing power oscillations generated by wind oscillation, or in a low-inertia microgrid [9]–[11]. FESSs have also been used for voltage sag mitigation in a shipboard power system [12]. However, less attention has been made to use of FESS in distribution networks and to our knowledge, real-time simulation of FESS has not to be published. Recently, the use High-Temperature Superconductors (HTS) bearings has led to signification reduction in losses in FESS[13]. However, till now, there is no use case of utilizing this new-generation FESS in power systems. In this paper, a FESS with High-Temperature Superconductive (HTS) bearings has been simulated in a real-time environment. The FESS is simulated in a Low Voltage (LV) distribution grid, supporting the loads during voltage sag and frequency disturbances. This is an essential step towards Hardware-in-the-Loop (HIL) testing and rapid prototyping of new controllers for the FESS and PHIL testing of parts or the whole the FESS itself.

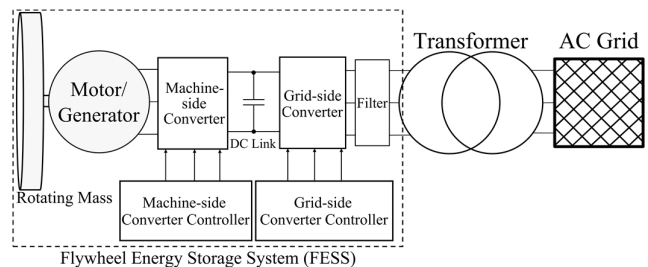


Fig. 1. The configuration of a grid-connected FESS.

In [14], a HIL testing of a new controller for a hybrid energy storage system consisting of Superconducting Magnetic Energy Storage (SMES) and Battery Energy Storage System (BESS) was conducted for microgrid applications, using its real-time models. Also, in [15], a hybrid flow-battery supercapacitor energy storage system, coupled with a wind turbine is simulated in real-time to smooth the power generated. In this work, the designed controller is embedded in a different real-time simulator.

This contribution is organized as follows. In section II, the FESS and its components are discussed with a focus on bearings technologies. Section III explains the modeling of the different components of the FESS. The real-time implementation and the results of model validation are presented in part IV.

II. THE CONFIGURATION OF A FESS

A Flywheel Energy Storage system (FESS) consists of several main components: a high-inertia rotor (i.e. the flywheel), an electrical machine, and back-to-back bi-directional power converters with a common DC link, converter controllers and a filter. The configuration of a conventional grid-connected FESS is illustrated in Fig. 1.

The rated power of a FESS is limited by the rated power of its electrical machine and the power converters, while its energy content is limited by the inertia of the rotor and its maximum rotational speed. The latter is restricted by the tensile strength of rotor materials, which has improved significantly in recent years by using composite fiber materials [16].

In a FESS, a higher energy density and lower losses are achieved by the use of magnetic bearings. In the following section, a short introduction to different bearing technologies for FESS applications is presented to discuss the use of HTS bearings. The flywheel can also rotate in a vacuum enclosure to remove the losses associated with air friction.

In general, FESS are grouped into two main categories, i.e. low-speed (less than 6000 rpm) and high-speed ($10^4 - 10^5$ rpm) FESS. A detailed comparison of differences between the two types of the flywheel is presented in TABLE I.

A. Bearings

Flywheel bearings support the weight of the rotor, keep it in position, damp out mechanical oscillations, and allow the free rotation with minimum losses. First generation flywheels use mechanical bearings, which results in high friction losses, lubrication requirements, and high maintenance cost. Magnetic bearings have been suggested as an alternative solution, in which the rotor is suspended in a magnetic field and a vacuum enclosure, eliminating friction losses and wearing. Therefore, they require much less maintenance and lower self-discharge rates are obtained. It is important to note that magnetic bearings lack friction losses, but other losses resulting from geometry and variance in a magnetic field, such as eddy current losses, leakage fluxes, and hysteresis are still present.

TABLE I. COMPARISON OF TWO TYPES OF FESS [17], [18]

Characteristic	Type of FESS	
	Low-speed FESS	High-speed FESS
Rotor Material	Steel	Composite Materials: Glass or Carbon Fiber
Electrical Machines Type	Asynchronous, Permanent magnet synchronous or reluctance machines	Permanent magnet Synchronous or reluctance machines
Integration of machine/flywheel	No integration or partial integration	Full or partial integration
Confinement atmosphere	A partial vacuum or light gas (Helium)	Absolute vacuum
Enclosure weight	$2 \times$ Flywheel weight	$\frac{1}{2} \times$ Flywheel weight
Bearings	Mechanical or hybrid (mechanical and magnetic)	Magnetic
Relative Capital Cost	1	5
Main Applications	Short-term and medium power applications	High power applications, Power quality and ride-through, ancillary services in power systems, Traction, and the aerospace industry
Specific Energy	~ 5 Wh/kg	~ 100 Wh/kg
Technology Maturity	Commercialized, Mature Technology	Early commercialization

Magnetic bearings themselves are categorized into active and passive bearings. Passive bearings use permanent magnets either alone or with a combination of High-Temperature Superconductors (HTS). HTS bearings have less intrinsic losses, compared to other types of magnetic bearings. Losses in a FESS with HTS bearings can be as low as 0.1% per hour, including the idle power [19]. Furthermore, the inhomogeneities and defects in HTS form the so-called pinning centers, which prevents the motion of flux lines until the Lorentz force exceeds some critical [20]. This keeps the flywheel rotor in balance and resists its movements. Therefore, it can be said that the rotor is self-stabilizing. In this study, a FESS with HTS bearings has been simulated. The structure of this system is shown in Fig. 2.

III. MODELING OF FLYWHEEL ENERGY STORAGE SYSTEMS

For the modeling of a FESS, detailed models of each component are mandatory and this includes, the Permanent Magnet Synchronous Machine (PMSM), two three-level voltage source converters, and their appropriate controllers.

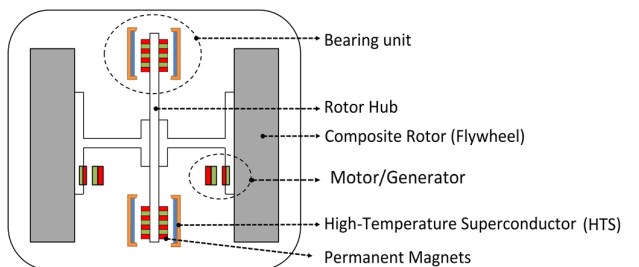


Fig. 2. The configuration of a high-speed FESS with HTS bearings.

A. Permanent Magnet Synchronous Machine (PMSM)

Permanent Magnet Synchronous Machines (PMSM) are the most common choice for high-speed flywheels. Because of the absence of field windings, it can easily be used in a vacuum enclosure. They also have a high power-to-weight ratio and a robust and simple structure, which leads to a higher reliability.

For modeling the PMSM the following assumptions have been made, which are all common assumptions for transient studies of electrical machines. The stator windings are identical and positioned sinusoidal along the air gap. As the flux generated by the permanent magnets in the stator is sinusoidal, the back-EMF is also sinusoidal. Hysteresis and saturation are neglected. In PMSMs eddy current losses are usually neglected, because the PMs are poor conductors and the eddy currents in nonmagnetic materials holding the PMs is very small [21].

The PMSM is modeled in the dq-rotating reference frame, which is aligned with rotating flux of the permanent magnets. With the mentioned simplifying assumptions, the PMSM in motor mode is modeled using the following equations [22].

$$u_d = r_s i_d + L_d \frac{di_d}{dt} - \omega_e L_q i_q \quad (1)$$

$$u_q = r_s i_q + L_q \frac{di_q}{dt} + \omega_e L_d i_d + \omega_e \quad (2)$$

$$T_e = \frac{3}{2} n_p (i_d i_q (L_d - L_q) + \psi_f i_{qm}) \quad (3)$$

$$J \frac{d\omega_m}{dt} = n_p (T_e - D\omega_m) \quad (4)$$

In the equations, u_d and u_q are the direct- and quadrature-axis stator voltages, i_d and i_q are the d- and q-axis stator currents, L_d and L_q are d- and q-axis stator inductances, r_s is the stator resistance, ω_e and ω_m are the electrical and mechanical speed, respectively, ψ_f is the permanent magnet flux, n_p is the number of pair poles, J is the rotor inertia, and D is the friction coefficient. Here, the friction factor is extremely small, since the FESS utilizes HTS bearings and it rotates in a vacuum enclosure. Also, a surface mounted PMSM is considered here, in which L_d and L_q are almost equal, resulting in a reluctance torque of zero.

B. Voltage Source Converters (VSC)

Depending on the intended study, different converter models can be selected based on the depth of details required for that particular study. This is of crucial importance for real-time simulations. In this paper, the average model has been used for the real-time simulation, since the behavior of the FESS from the grid perspective and after the filters is of interest. The average model has the shortest computation time, since the switching transitions, harmonics, and ripples are removed by averaging over one switching period. Nevertheless, the slower variation of the variables is preserved. In the averaged model, and the VSC is modeled as

a three-phase controlled AC voltage source with a small internal resistance as shown in Eq. (5) [23].

$$u_j = m_j \frac{U_D}{2} - r_o i_j \quad (5)$$

In which j denotes to the three phases, a, b, and c, m_j is the modulation index, U_D is the voltage of the DC-side, and u_j and i_j are the voltage and current of the AC-side, respectively, and r_{on} represent the on-state resistance of VSC switch cells. Also, for a lossless converter in linear modulation operation, it can be written,

$$P_A = \sum_{j=a,b,c} u_j i_j = U_D I_D = P_D \quad (6)$$

C. Grid-side Converter Controller.

The Grid-side Converter (GSC) controls the active and reactive power exchanged between the FESS and the grid. It also has the task of voltage and frequency regulation. To avoid the operation of the FESS in insignificant disturbances, a deadband has been considered for both voltage and frequency error. The AC-side instantaneous voltage is calculated using a rotating frame, which enables immediate detection of any changes in the voltage. To prevent high transient currents, an internal current controller is usually added for such systems. It is assumed that the dq-frame for the GSC converter is chosen in a way that the AC-side voltage of the GSC is in alignment with d-axis. The Phase-Locked Loop (PLL) maintains the value of the q-axis component of the grid voltage to zero. By doing so and according to Eq. (7) and (8), active and reactive power can then be controlled separately, by adjusting the values of i_d and i_q , respectively.

$$P_g = \frac{3}{2} (u_d i_d + u_q i_q) \quad (7)$$

$$Q_g = \frac{3}{2} (-u_d i_q + u_q i_d) \quad (8)$$

The frequency and voltage control are designed with a droop-based approach. The droop setting for frequency control determines how much the active power of the FESS should change in response to a change in frequency, which may differ for positive and negative frequency errors in this design. For the internal current controllers, a feedforward has been added to reduce the high transient current during start-up, which also decouples dynamics of the converter system from those of the AC system and improves its disturbance rejection capability [23]. The outputs of the PI current controllers have been added with a decoupling factor in order to enable an independent control of the d-axis and q-axis current.

D. Machine-side Converter

The machine-side converter controls the PMSM and at the same time maintains the DC-side voltage. This is done by controlling the amplitude and phase of the output voltage of the MSC via the modulation indices. For controlling the PMSM, the maximum torque per Ampere is used, in which

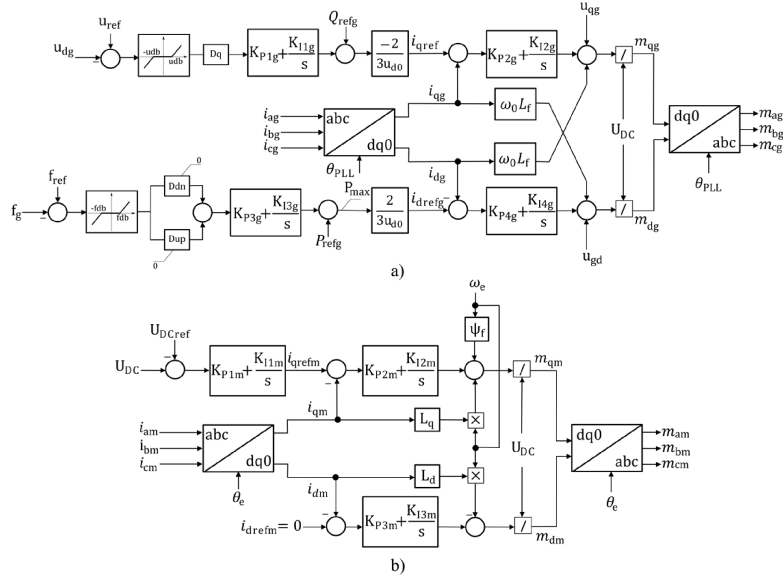


Fig. 3. Converter Controller Design for a) Grid-side Converter b) Machine-side Converter.

the objective is to force the d-axis current to zero. This results in maximum electrical torque with same stator current, as shown in Eq. (3).

Parameters for the PMSM, converters and the controllers can be found in the appendix. The controller design for both the MSC and the GSC is illustrated in Fig. 3.

IV. REAL-TIME SIMULATION RESULTS

A. Implementation in a Real-time Simulation Environment

All real-time simulations have been carried out on the Opal-RT's OP5600 digital real-time simulator using the Linux-based Hypersim software. Hypersim, originally developed by the Hydro-Quebec's research institute (IREQ), enables a nonlinear solver for real-time simulation, which uses the trapezoidal rule of integration as the main numerical method for solving the ODEs [39], [40].

In this work, the real-time simulation of the studied system including the all the components illustrated in Fig. 4 is achieved with simulation steps of only 10 microseconds.

B. Model Validation.

To validate the model of the FESS in Hypersim, the exact model of the system shown in Fig. 4 including all the components have also been implemented in MATLAB. The trapezoidal rule has been used as the numerical solver method to avoid inaccuracies due to the solver selection. This also improves the numerical stability of the simulations.

As shown in Fig. 4, the FESS is connected to a medium voltage of a grid via a 0.4/20 kV transformer. For the AC grid, a short-circuit capacity of 100 MVA and X/R ratio of 1 has been considered [31]. The FESS is also supporting a critical load, representing an industrial facility. The model validation has been done by simulating voltage dips and reference step

responses. The results of a selection of the scenarios are presented in this paper.

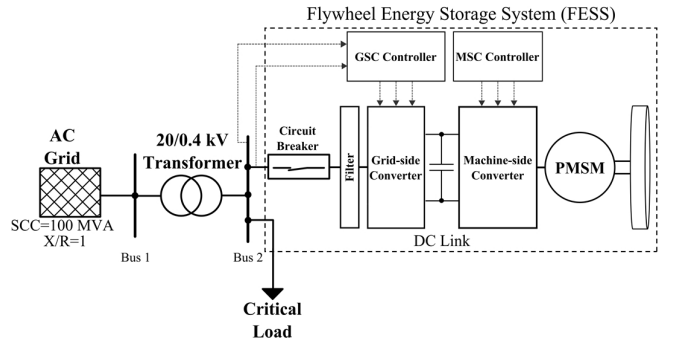


Fig. 4. Single line diagram of the simulated system.

1) Frequency step response.

In this test, the reference value for the frequency at the GSC controller has been altered from 50 Hz to 51 Hz and response of the FESS and its controllers has been analyzed. Since the FESS is connected to a rigid grid, obviously it cannot change the grid frequency. However, the FESS should support the network by increasing its active power output according to its droop settings. Here, a 20% increase in power per Hertz for a 100 kW FESS is expected. The results of the real-time simulation for this scenario has been shown in Fig. 5. As shown, the FESS injects 20 kW to the network and reaches steady-state conditions in less than a cycle. By injecting active power to the grid, the DC link voltage will start to fall. However, the MSC controller immediately reacts and recovers the DC link voltage to the initial value. This is done by drawing q-axis current from the PMSM, which leads to negative electrical torque and decrease of flywheel speed.

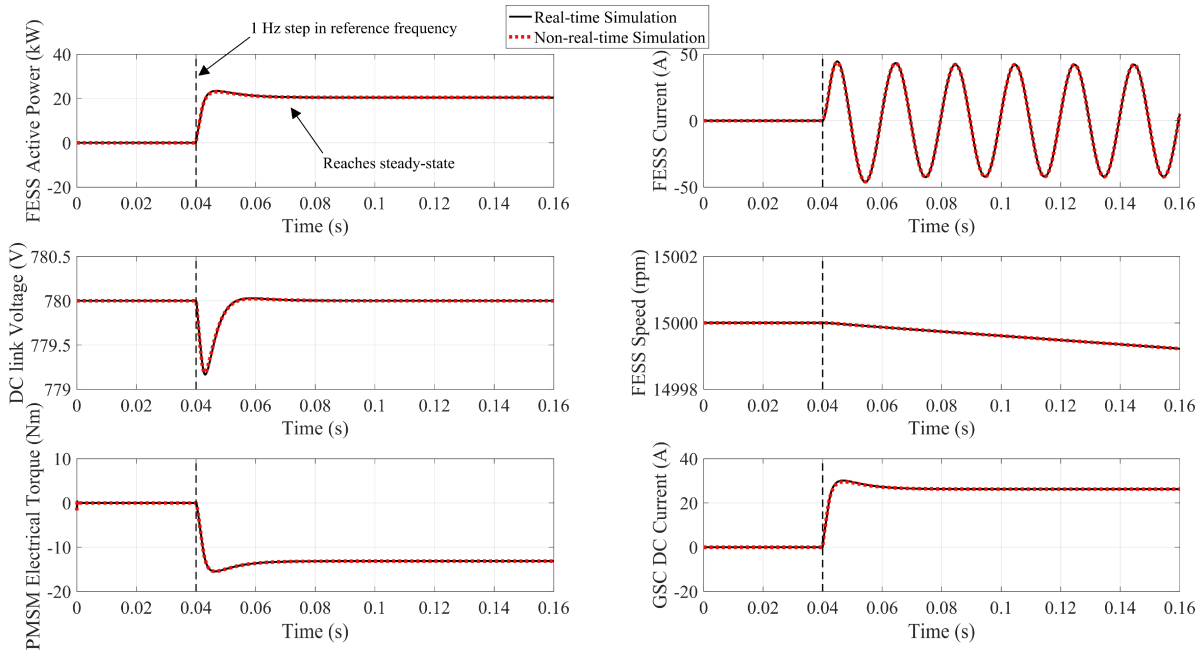


Fig. 5. Validation of the FESS real-time model with a 1 Hz change in the reference frequency.

The FESS is initially fully charged at 15000 rpm. The speed of the flywheel will start to decrease, but because of the short observation time and the extremely high inertia of the rotor, only a slight decrease is observed in Fig 5.

2) Voltage sag response.

Voltage sags with various depth of 5, 10, 15 and 20% have been simulated in AC grid. Such voltage dips are common and could be caused by faults in the high voltage networks or other parallel feeders. For all the simulated cases, the reactive power compensation by the FESS is shown in Fig. 6. The detailed results for the 20% voltage dip are illustrated in Fig. 7

Since in this scenario, mostly reactive power injection is required, there are no significant changes in the PMSM mechanical speed. Here, the FESS acts similar to a static compensator (STATCOM). Only a small active power is provided by the FESS to compensate for the on-state losses of the converter and the losses in the filter. Moreover, since the FESS operates in a distribution network with relatively low X/R ratio, the active and reactive power are not fully decoupled, as in a transmission network.

As illustrated, the results of the real-time simulation have an acceptable match with the non-real-time simulations in both transient and steady-state values.

C. Possible Applications.

As mentioned earlier, the real-time simulation enables the interaction of the model with the hardware. This can be done by the I/O port of the Opal-RT's real-time simulator. Therefore, a controller prototype for GSC or MSC or both can be designed and built and its effectiveness in controlling of the FESS can be tested with the real-time model. New PMSMs or new converters can also be tested via this

platform. However, in case of hardware integration, the communication overheads should be added in the simulation step size.

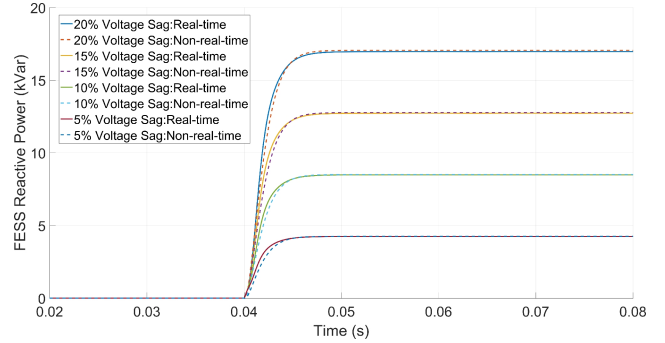


Fig. 6. Reactive power compensation by the FESS during different voltage sag levels.

V. CONCLUSION

In this paper, a High-speed Flywheel Energy Storage System (FESS) with HTS bearings has been modeled in details and simulated in real-time. A controller design based on the required ancillary services required in the LV network has been suggested. The results of the real-time simulation have been verified by non-real-time simulations and a good match in the transient behavior of the system has been observed. The real-time simulation not only excels the speed of the simulation, but also enables the interaction of the model with real hardware. Such a platform can later be used for testing and prototyping of different controller design, as well as acting as the base case for PHIL simulation of FESS.

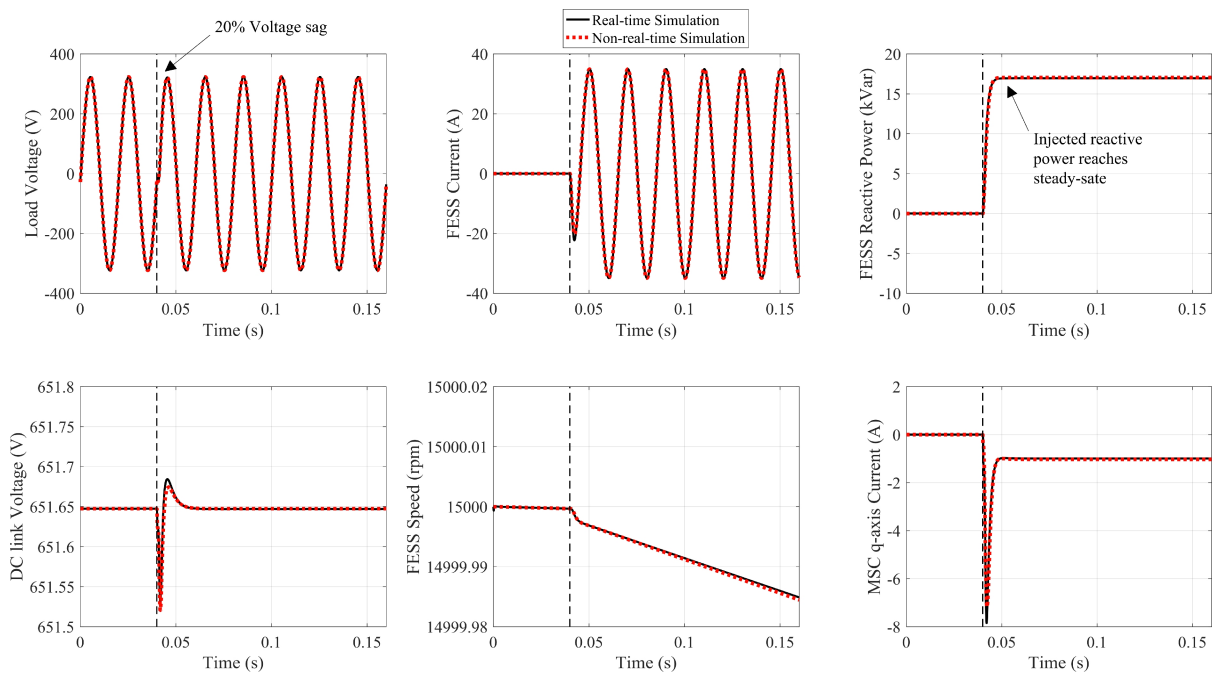


Fig.7. Validation of the FESS real-time model with a 20% voltage sag from the grid-side.

ACKNOWLEDGMENT

This work was supported by the German Research Foundation (DFG) as part of the Research Training Group GRK 2153: Energy Status Data - Informatics Methods for its Collection, Analysis, and Exploitation.

VI. REFERENCES

- [1] M. D. Omar Faruque *et al.*, "Real-Time Simulation Technologies for Power Systems Design, Testing, and Analysis," *IEEE Power Energy Technol. Syst. J.*, vol. 2, no. 2, pp. 63–73, 2015.
- [2] R. Venugopal, W. Wang, and J. Belanger, "Advances in real-time simulation for power distribution systems," *2011 Int. Conf. Energy. Autom. Signal*, pp. 1–6, 2011.
- [3] T. F. Stocker *et al.*, "Technology Roadmap: Energy Storage," 2014.
- [4] S. Ghosh and S. Kamalasan, "An Integrated Dynamic Modeling and Adaptive Controller Approach for Flywheel Augmented DFIG Based Wind System," *IEEE Trans. Power Syst.*, vol. 8950, pp. 1–1, 2016.
- [5] G. O. Suvire and P. E. Mercado, "Active power control of a flywheel energy storage system for wind energy applications," *Renew. Power Gener. IET*, vol. 6, no. 1, pp. 9–16, 2012.
- [6] G. Cimuca, S. Breban, M. M. Radulescu, C. Saudemont, and B. Robyns, "Design and control strategies of an induction-machine-based flywheel energy storage system associated to a variable-speed wind generator," *IEEE Trans. Energy Convers.*, vol. 25, no. 2, pp. 526–534, 2010.
- [7] L. Wang and C. T. Hsiung, "Dynamic stability improvement of an integrated offshore wind and marine-current farm using a flywheel energy-storage system," *IEEE Trans. Power Syst.*, vol. 26, no. 2, pp. 690–698, 2011.
- [8] F. Islam, A. Al-Durra, and S. M. Mueen, "Smoothing of wind farm output by prediction and supervisory-control-unit-based FESS," *IEEE Trans. Sustain. Energy*, vol. 4, no. 4, pp. 925–933, 2013.
- [9] F. Diaz-Gonzalez, A. Sumper, O. Gomis-Bellmunt, and R. Villafila-Robles, "Modeling and Validation of a Flywheel Energy Storage Lab-Setup," *2012 3rd IEEE PES Innov. Smart Grid Technol. Eur. (ISGT Eur.)*, pp. 1–6, 2012.
- [10] N. Hamsic *et al.*, "Stabilising the Grid Voltage and Frequency in Isolated Power Systems Using a Flywheel Energy Storage System," *Gt. Wall World Renew. Energy Forum*, no. October, pp. 1–6, 2006.
- [11] "Program on Technology Innovation: Microgrid Implementations: Literature Review 2016," Palo Alto, California, 2016.
- [12] S. Samineni, B. K. Johnson, H. L. Hess, and J. D. Law, "Modeling and Analysis of a Flywheel Energy Storage System with a Power Converter Interface," vol. 4, no. 1, pp. 2–7, 2003.
- [13] M. Strasik *et al.*, "An overview of Boeing flywheel energy storage systems with high-temperature superconducting bearings," *Supercond. Sci. Technol.*, vol. 23, no. 3, p. 34021, 2010.
- [14] H. K. Ji, H. J. Yoo, and H. M. Kim, "Performance test of coordinated control of SMES and BESS in microgrid using the hardware-in-the-loop simulation system," *Int. J. Control Autom.*, vol. 8, no. 3, pp. 161–170, 2015.
- [15] W. Li, G. Joos, and J. Belanger, "Real-Time Simulation of a Wind Turbine Generator Coupled With a Battery Supercapacitor Energy Storage System," *IEEE Trans. Ind. Electron.*, vol. 57, no. 4, pp. 1137–1145, 2010.
- [16] M. A. Conteh and E. C. Nsofor, "Composite flywheel material design for high-speed energy storage," *J. Appl. Res. Technol.*, vol. 14, no. 3, pp. 184–190, 2016.
- [17] S. M. Mousavi G, F. Faraji, A. Majazi, and K. Al-Haddad, "A comprehensive review of Flywheel Energy Storage System technology," *Renew. Sustain. Energy Rev.*, vol. 67, pp. 477–490, 2017.
- [18] B. Bolund, H. Bernhoff, and M. Leijon, "Flywheel energy and power storage systems," *Renew. Sustain. Energy Rev.*, vol. 11, no. 2, pp. 235–258, 2007.
- [19] M. Strasik *et al.*, "Design, fabrication, and test of a 5-kWh/100-kW flywheel energy storage utilizing a high-temperature superconducting bearing," *IEEE Trans. Appl. Supercond.*, vol. 17, no. 2, pp. 2133–2137, 2007.
- [20] T. Matsushita, *Flux Pinning in Superconductors*, 2nd ed. Springer Science, 2007.
- [21] P. C. Krause, O. Wasynczuk, and S. D. Sudhoff, *Analysis of Electric Machinery and Drive Systems*. 2002.
- [22] Ion Boldea and L. N. Tutelea, *Electric Machines: Steady State, Transients, and Design with MATLAB*. CRC Press, 2009.
- [23] A. Yazdani and R. Iravani, *Voltage-Sourced Converters in Power Systems*. New Jersey: John Wiley & Sons, Inc, 2010.

A- APPENDIX

The parameters used in the simulation of the FESS and its components for the real-time and non-real-time simulation is presented in TABLE A-1.

TABLE A-1. The parameters of the simulation of the FESS.

Description	Parameter	Value
PMSM		
Stator Resistance	r_s	2.2 m Ω
d-axis Inductance	L_d	7 μ H
q-axis Inductance	L_q	7 μ H
Permanent Magnet Flux	ψ_f	0.288 Wb
Number Poles	n_p	3
Inertia	J	19.8 Kg.m ²
Friction Coefficient	D	1.1×10^{-5}
VSC		
On-state Resistance	r_o	0.88 m Ω
DC Link Capacitance	C	6 mF
GSC		
AC-side Voltage Controller - Proportional Term	K_{P1g}	1
AC-side Voltage Controller - Integral Term	K_{I1g}	30000
Voltage Droop Setting	Dq	0.1
q-axis Current Controller- Proportional Term	K_{P2g}	5
q-axis Current Controller- Integral Term	K_{I2g}	10
Frequency Droop Setting	Dup, Ddn	20,000
Frequency Controller - Proportional Term	K_{P3g}	1
Frequency Controller - Integral Term	K_{I3g}	0.1
d-axis Current Controller- Proportional Term	K_{P4g}	0.1
d-axis Current Controller- Integral Term	K_{I4g}	10
MSC		
DC-side Voltage Controller - Proportional Term	K_{P1m}	10
DC-side Voltage Controller - Integral Term	K_{I1m}	3000
q-axis Current Controller- Proportional Term	K_{P2m}	2
q-axis Current Controller- Integral Term	K_{I2g}	1000
d-axis Current Controller- Proportional Term	K_{P3m}	2
d-axis Current Controller- Integral Term	K_{I3m}	1000
Filter		
Resistance of the Filter	-	1 m Ω
Inductance of the Filter	-	0.2 mH